JACS
JOURNAL OF THE AMERICAN CHEMICAL SOCIETY
Communication
pubs.acs.org/JACS

Bubble-Free Propulsion of Ultrasmall Tubular Nanojets Powered by Biocatalytic Reactions

Xing Ma,[‡,#] Ana C. Hortelao,[‡,∥] Albert Miguel-López,[∥] and Samuel Sánchez*[,‡,∥,§]

[‡]Max-Planck Institute for Intelligent Systems Institution, Heisenbergstraße 3, 70569 Stuttgart, Germany
[#]School of Materials Science and Engineering, Harbin Institute of Technology Shenzhen Graduate School, 518055 Shenzhen, China
[∥]Institut de Bioenginyeria de Catalunya (IBEC), Baldiri i Reixac 10-12, 08028 Barcelona, Spain
[§]Institució Catalana de Recerca i Estudis Avancats (ICREA), Pg. Lluís Companys 23, 08010 Barcelona, Spain

Supporting Information

ABSTRACT: The motion of self-propelled tubular micro- and nanojets has so far been achieved by bubble propulsion, e.g., O_2 bubbles formed by catalytic decomposition of H_2O_2, which renders future biomedical applications inviable. An alternative self-propulsion mechanism for tubular engines on the nanometer scale is still missing. Here, we report the fabrication and characterization of bubble-free propelled tubular nanojets (as small as 220 nm diameter), powered by an enzyme-triggered biocatalytic reaction using urea as fuel. We studied the translational and rotational dynamics of the nanojets as functions of the length and location of the enzymes. Introducing tracer nanoparticles into the system, we demonstrated the presence of an internal flow that extends into the external fluid via the cavity opening, leading to the self-propulsion. One-dimensional nanosize, longitudinal self-propulsion, and biocompatibility make the tubular nanojets promising for future biomedical applications.

Researchers have fabricated multiple micro/nanomotors that mimic natural systems[1] and are capable of converting chemical energy into kinetic energy for self-propulsion.[2] Tubular catalytic motors have been demonstrated as versatile "on-the-fly" microsystems for various proof-of-concept applications, such as heavy metal capture[3] or water remediation,[4] cargo loading and transportation,[5] drug delivery,[6] sensing,[7] and as microdrillers for minimally invasive surgery.[8] Almost all the current tubular motors are driven by a bubble propulsion mechanism on the micrometer scale. Usually, an inorganic catalytic component, such as platinum,[6,9] silver,[10] or MnO_2,[11] is included inside the tubes to trigger decomposition of hydrogen peroxide ($H_2O_2 \rightarrow H_2O + {}^1/_2O_2$). Alternatively, catalase enzyme has been used as an organic catalyst to efficiently provide self-propulsion by decomposing much lower concentrations of H_2O_2.[7b,12] The underlying mechanism involves the formation and continuous ejection of oxygen bubbles from the tubular confinement, provoking motion in the opposite direction.

Before now, there have been two major strategies for the fabrication of tubular motors. One is the "rolling-up" method based on clean-room photolithography and electron-beam evaporation techniques, which can produce tubular structures with sizes from sub-micrometer up to 30 μm diameter and from 25 μm to 1 mm length.[8a,9b,13] Clean-room-free "rolling-up" methods have been also reported.[14] The other method is electrochemical deposition on porous membranes (Al_2O_3 or polycarbonate),[3,7b,9a] which produces microtubes from 2 to 5 μm diameter. Until now, only a very few works have reported nanotubular motors, all of them using high concentrations of H_2O_2 as fuel and surfactant to reduce the surface tension.[8a,14,15] A cheap and facile fabrication method that could be scaled-up, enabling a metal-free nanoarchitecture, is sought. Biofriendly processes such as enzyme catalysis can provide mechanical force to drive micro/nanostructures, with great potential for biocompatible self-powered systems.[16] We previously demonstrated that enzyme-based silica micromotors show biocompatibility against HeLa cells.[16e] Additionally, a bubble-free propulsion mechanism would avoid accumulation of gas bubbles in the fluidic environment, which is advantageous for future *in vivo* biomedical use.

Herein, we present ultrasmall tubular silica nanojets (220 nm diameter on average) that are self-propelled by enzymatic reactions. The nanojets are powered by the turnover of urea substrate (at physiological concentrations) triggered by enzyme urease (urea $\rightarrow NH_{3(aq)} + CO_{2(aq)}$). The reaction products, ammonia and carbon dioxide, are formed inside the nanotubes (NTs), generating internal flows that extend into the external space via the tube opening. This generates a thrust longitudinally that maintains the directional movement of the nanojets by a "jetting effect".[17] The existence of a flow was supported by analyzing tracer nanoparticles (NPs) expelled from the back side of the nanojets.

The silica nanotubes (SNTs) were fabricated by using silver nanowires (AgNWs, 115 nm × 50 μm) as the templates on which a thin layer of silica was grown by sol−gel chemistry.[18] The silica-coated AgNWs (AgNW@SiO_2) (Figure S1a) were then broken down into shorter segments by sonication for 3 h (see details in the Supporting Information (SI)). After removal of the AgNW templates by etching in *aqua regia* overnight, the SNTs were obtained (Figure S1b,c). We functionalized the SNTs with amine groups (-NH_2) by grafting, yielding SNT-NH_2. The amine groups on SNT-NH_2 were detected by fluorescamine, which upon reaction with primary -NH_2 exhibit fluorescent emission at 477 nm (Figure S2a). Zeta-potential measurement showed that the

Received: July 3, 2016
Published: October 9, 2016

DOI: 10.1021/jacs.6b06857
J. Am. Chem. Soc. 2016, 138, 13782−13785

surface charge of the SNTs changed from −39 ± 11 to 44 ± 11 mV for SNT-NH_2, proving the success of surface functionalization with amine groups (Figure S2b). We further conjugated enzyme (urease) onto the surface of the SNTs by using glutaraldehyde as a linker molecule,[16e,f] yielding SNT-urease (Figure 1a). We

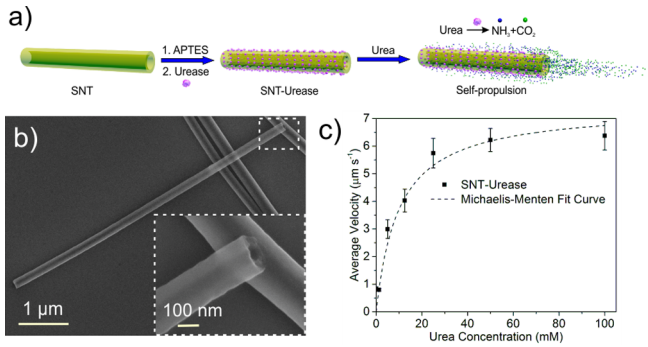

Figure 1. (a) Schematic illustration of the fabrication of urease-conjugated silica tubular (SNT-urease) nanojets. (b) Typical SEM image of the SNTs. (c) Fuel-dependent average velocity of SNT-urease with an average length of 10 μm. Error bars indicate standard error of the mean, N = 10.

confirmed the enzyme conjugation by using a protein staining kit to visualize the presence of urease on the SNT-urease, as indicated by red fluorescence color in Figure S3.[16e] A typical scanning electron microscopy (SEM) image of a SNT is presented in Figure 1b, and its quasi-transparent tubular structure in the inset image. The average diameter of the SNTs, determined from SEM images, is D = 220 ± 24 nm (average ± standard deviation, N = 30). The length of the NTs ranges from 3 to 40 μm and can be controlled by using different templates, centrifugation, and variable sonication times. When the enzymatic nanojets were placed in solution containing urea, we observed directional self-propulsion along the longitudinal axis (Video S1). The average velocity of tubular nanojets with an average length of ∼10 μm (9−13 μm) showed a fuel-dependent increasing trend, which fits well with the Michaelis−Menten enzymatic kinetics, reaching a plateau at 25 mM (Figure 1c). The close correlation between velocity and enzymatic activity suggests that the biocatalytic reaction provides mechanical power for the motion of the nanojets.

In the absence of urea, the nanojets exhibited only Brownian motion (Figure S4 and Video S2). The translational diffusion coefficient (D_t) retrieved from a mean-square displacement (MSD) plot (MSD = $4D_t\Delta t$ for two-dimensional case) fits well with the theoretical calculation (inset of Figure 2b).[19] Upon addition of urea (100 mM), the nanojets showed longitudinal self-propulsion. Snapshots of tracking trajectories of the self-propelled nanojets of three different lengths (3.17, 5.42, and 18.03 μm) are presented in Figure 2a (Video S3). We characterized the motion of the nanojets by quantifying the velocity (V), measuring the longitudinal displacement (ΔL) within a given time (Δt), as $V = \Delta L/\Delta t$. We found a decreasing trend of the velocity with increasing length of the nanojets (Figure 2b). We further analyzed the rotational diffusion of the nanojets by automatic tracking of the orientation angle (θ) of the nanojets, as shown in Video S1 and Figure S5a. The plot of mean square angular displacement (MSAD) was calculated to retrieve the effective rotational diffusion coefficient D_r(eff) by the equation MSAD = $2D_r(\text{eff})\Delta t$ in the one-dimensional case, as shown in Figure S5c.

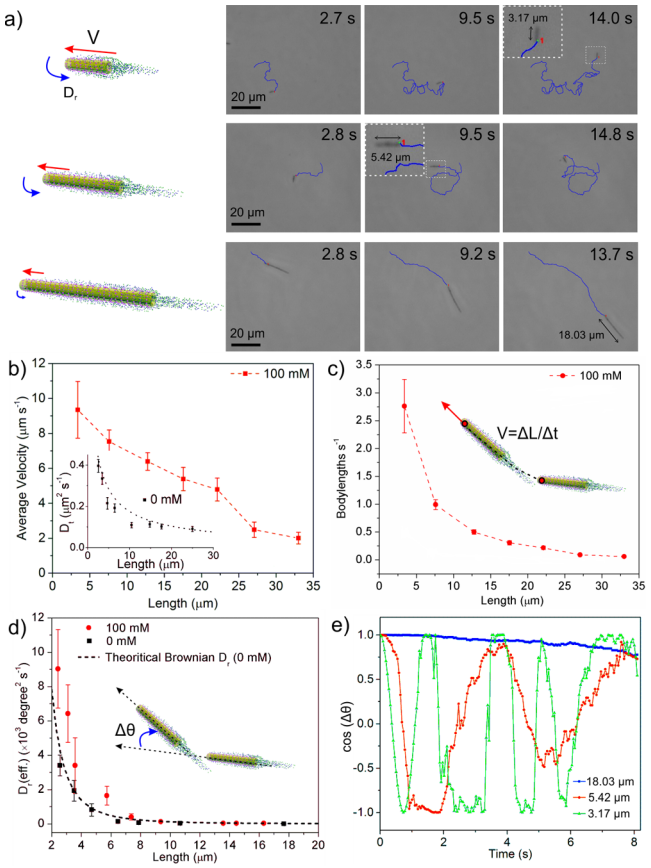

Figure 2. Dynamics of urease-powered tubular nanojets. (a) Schematic illustration and tracking trajectories of the tubular nanojets with varied lengths. Variation with tubular nanojet length of (b) longitudinal average velocity in μm s^{-1} (inset is Brownian translational diffusion coefficient, D_t, of the nanojets without fuel; dashed line is theoretical value of D_t), (c) body lengths in s^{-1}, and (d) effective rotational diffusion coefficient (D_r(eff)) with (100 mM) and without (0 mM) fuel (dashed line is theoretical value of Brownian D_r). (e) Angular autocorrelation of the three nanojets shown in (a). Error bars indicate standard error of the mean, N = 10.

In the absence of fuel, the rotational diffusion of the nanojets was only due to Brownian motion, consistent with the theoretical calculation (dashed line, Figure 2d).[19] In the presence of urea, the tubular nanojets showed enhanced rotational diffusion, in particular when their length was <10 μm. However, the rotational behavior was stabilized and angular changes decreased when the length of the tubular motors was >10 μm. To learn more details about the orientation change with time of three distinct nanojets, we analyzed their angular autocorrelation (cos($\Delta\theta$)) for a period of 8 s, where $\Delta\theta$ is the angular change compared to their initial orientation,[20] as plotted in Figure 2e. A quickly changing autocorrelation value indicates a fast rotation of the nanojets, whereas a constant value close to 1 is associated with a stable orientation. The frequency of angular change for the nanojet of length 3.17 μm is substantially higher than that for the 5.42 μm one (green and red lines, respectively). A nanojet of ∼18 μm (blue line) maintains an undisturbed angular correlation for the represented time.

To identify the driving force of the nanojets, we selectively functionalized urease inside (SNT-Urease-I), outside (SNT-Urease-O), or all over the nanotube (SNT-Urease-A), as presented in Figure 3a (see experimental procedures in the SI).

DOI: 10.1021/jacs.6b06857
J. Am. Chem. Soc. 2016, 138, 13782−13785

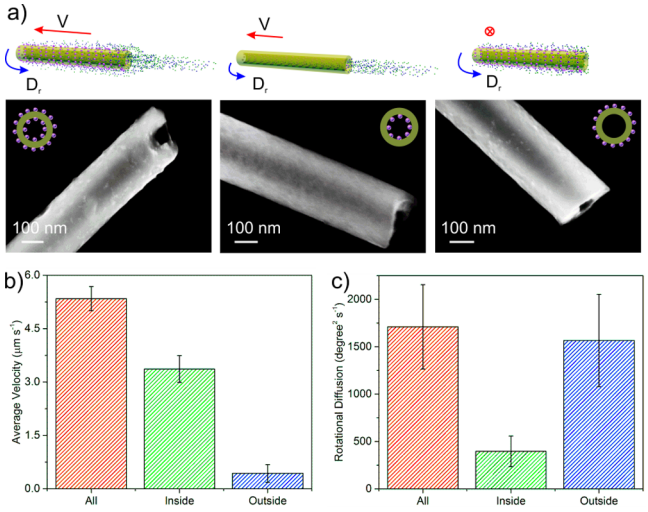

Figure 3. Enzyme location-dependent motion behavior. (a) Schematic illustration of SNT-urease with enzyme all over (SNT-urease-A), inside (SNT-urease-I), and outside (SNT-urease-O) the nanotube, and corresponding SEM images. (b) Longitudinal average velocity of the three nanotubular motors with average length of 20 μm. (c) Rotational diffusion of the three nanotubular motors with average length of 5.5 μm. Error bars indicate standard error of the mean, $N = 10$.

The presence of urease on the external surface of the samples of SNT-Urease-A and SNT-Urease-O was seen in the SEM images (Figure 3a), while smooth bare silica was observed for SNT-Urease-I. The protein concentration conjugated to the different types of NTs was evaluated using a Coomassie Brilliant Blue-based protein quantification kit (Figure S10a). Furthermore, the enzymatic activity of the three urease-conjugated tubular nanojets was evaluated according to a previously reported method,[16f] indicating that the immobilized enzymes on all three nanojets were active (Figure S10b).

The effect of enzyme location on the dynamics of the three types of nanojets with average length of 20 μm was analyzed (Figure 3b). Although all three nanojets were biocatalytically active, only SNT-Urease-A and SNT-Urease-I demonstrated longitudinal self-propulsion (Video S4). In contrast, SNT-Urease-O showed only Brownian motion. These results evidence that the longitudinal self-propulsion of the tubular nanojets should be attributed to the enzymatic reaction taking place inside the NTs. SNT-Urease-A has the highest velocity among the three tubular nanojets, implying that the enzymatic reactions on the external surface might contribute to enhancing the longitudinal velocity. The change from silica/H_2O molecules on a nonactive surface into a much more complex situation, where interactions between multiple molecules (e.g., biocatalytic products) and the enzymatically active surface of SNT-Urease-A were taking place, might alter the interfacial tension and possibly decrease resistance to self-propulsion, leading to velocity enhancement. We tracked tracer NPs located near the nanojets and found that those were "attracted" toward the outer surface, implying a flow field on the surface of the nanojet. Similarly to the enzymatic micropumps reported by Sen et al.,[21] the enzymatically active outer surface would create density-driven convective flows that can be indirectly observed by the "trapping" effect of tracer NPs along the tube surface (see details in Figure S11 and discussion in the SI). Such an external flow field might also contribute to the velocity enhancement for the SNT-Urease-All. However, further in-depth investigation is needed before reaching a conclusive understanding of this phenomenon.

We further analyzed the rotational behavior of the three kinds of nanojets with an average length of 5.5 μm, at which an obvious nonbalance effect was observed. SNT-Urease-A and SNT-Urease-O showed 3 times higher rotational diffusion coefficients compared to SNT-Urease-I (Figure 3c), suggesting that the enzymatic reaction on the external surface of the tubular nanojets indeed enhanced their rotational diffusion.

The biocatalytic nanojets act as jet engines as they generate thrust from their cavity, releasing a jet of fluid backward (in this case the products of the enzymatic reaction). Before now, this jetting force provided by catalytic microjets has been caused by bubble generation. In the current work, the products do not generate visible bubbles, yet they induce enough propelling force to move the nanojets forward. This jet of liquid has been studied using a suspension of tracer NPs with the nanojets (Figure 4 and

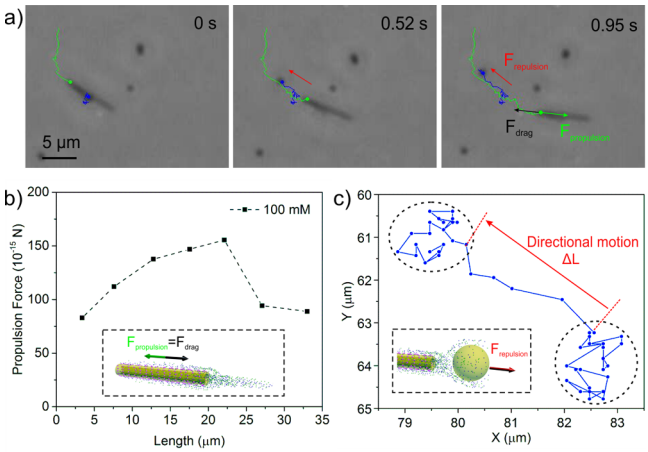

Figure 4. Nanopropulsion from internal flows. (a) Video snapshot of a self-propelled nanojet (green track) expelling a tracer NP (blue tracking trajectory). (b) Propulsion force of the nanojets calculated by eq 2, based on the velocity value in Figure 2b. (c) Tracking trajectory of the tracer NP indicates the directional motion of the tracer NP instantly pushed by the repulsion force originated from the internal flow.

Video S5). The tracking trajectory is presented in Figure 4a. At low Reynolds numbers, the propulsion force (F_{prop}) is equal to the drag force (F_{drag}) applied on the tubular nanojets,[22] as indicated in Figure 4a. We approximated the dynamics of the tubular nanojets by using the Stokes' drag equation for nanorods,[9a,23]

$$F_{drag} = \frac{2\pi\mu LV}{\ln(2L/R) - 0.72} \quad (1)$$

where μ is viscosity and R, L, and V are radius, length, and velocity of the nanorods, and we calculated the drag force applied on the tubular nanojets based on the velocity results presented in Figure 2c. As shown in Figure 4b, the drag force ranges from 80 to 150 fN. When the NPs were not affected by the flow field of the active nanojets, they demonstrated only randomized Brownian motion (blue trajectory) without any given directionality. The tracer NPs, once in the vicinity of the rear opening of nanojets, were repelled and pushed away, which clearly evidenced the internal flow of the biocatalytic products (Figure 4c). We measured the length (ΔL = 4.07 μm) and time interval (Δt = 0.21 s) of the directional motion range of the specific tracer NP in Figure 4a and calculated the instantaneous velocity of the tracer NP as $V = \Delta L/\Delta t$ = 19.38 μm s^{-1}. By Stokes' drag law for an active spherical particle in fluid,

DOI: 10.1021/jacs.6b06857
J. Am. Chem. Soc. 2016, 138, 13782−13785

$$F = 6\pi\mu RV \quad (2)$$

where μ is viscosity and R and V are radius and velocity of the particle, we calculated the drag force (F_{drag}(NP) = 124 fN) during the directional motion range, which can be used to approximate the repulsion force F_{rep}(NP) applied on the tracer NP. The length and the longitudinal velocity of the specific tubular nanojet shown in Figure 4a are L = 6.93 μm and V = 9.58 μm s^{-1}. Thus, the drag force (propulsion force) for the specific tubular nanojet was found to be F_{drag}(jet) = F_{prop}(jet) = 134 fN (by eq 1), which agrees with the repulsion force (or drag force) of the tracer NP found experimentally. These results prove that the motion of the tubular nanojets can be attributed to active flow of the enzymatic reaction products, providing a new mechanism for tubular motors besides the current bubble propulsion mechanism.

In summary, we fabricated a self-propelled tubular nanojet driven by a bubble-free propulsion mechanism. In contrast to most tubular motors based on bubble propulsion by decomposition of H_2O_2, the mechanical power is generated by enzymatic decomposition of biofriendly urea substrate that does not generate visible bubbles. We observed that not only enzymes inside but also those located outside the nanojets contribute to the self-propulsion. Considering the small dimension and biofriendly motors and fuel, these nanojets hold great potential for use in biomedical fields. To control their motion, the use of external sources will be necessary as well as the study of the collective behavior of nanojets. Further experimental and theoretical studies will be performed to better understand the non-bubble propulsion mechanism.

■ ASSOCIATED CONTENT

Supporting Information

The Supporting Information is available free of charge on the ACS Publications website at DOI: 10.1021/jacs.6b06857.

Experimental details of protocols, methods, and characterization, including Figures S1−S11 (PDF)

Video S1, self-propulsion of SNT-urease; Video S2, SNT-urease at 0 mM urea; Video S3, SNT-urease of varied length at 1000 mM urea; Video S4, SNT-urease with enzyme all over, inside, and outside; and Video S5, moving SNT-urease with tracer NPs (AVI)

■ AUTHOR INFORMATION

Corresponding Author

*sanchez@is.mpg.de; sanchez@ibecbarcelona.eu

Notes

The authors declare no competing financial interest.

■ ACKNOWLEDGMENTS

The research leading to these results has received funding from the European Research Council under the European Union's Seventh Framework Program (FP7/20072013)/ERC grant agreement no. 311529 (LT-NRBS) and the Alexander von Humboldt Foundation (to X.M.). S.S. thanks the Spanish MINECO for grants CTQ2015-68879-R (MICRODIA) and CTQ2015-72471-EXP (Enzwim).

■ REFERENCES

(1) (a) Sánchez, S.; Soler, L.; Katuri, J. *Angew. Chem., Int. Ed.* **2015**, *54*, 1414. (b) Wang, H.; Pumera, M. *Chem. Rev.* **2015**, *115*, 8704. (c) Wang, J. *Nanomachines: Fundamentals and Applications*; Wiley- VCH: Weinheim, 2013. (d) Lin, X.; Wu, Z.; Wu, Y.; Xuan, M.; He, Q. *Adv. Mater.* **2016**, *28*, 1060.

(2) (a) Sengupta, S.; Ibele, M. E.; Sen, A. *Angew. Chem., Int. Ed.* **2012**, *51*, 8434. (b) Ozin, G. A.; Manners, I.; Fournier-Bidoz, S.; Arsenault, A. *Adv. Mater. (Weinheim, Ger.)* **2005**, *17*, 3011. (c) Paxton, W. F.; Sundararajan, S.; Mallouk, T. E.; Sen, A. *Angew. Chem., Int. Ed.* **2006**, *45*, 5420.

(3) Vilela, D.; Parmar, J.; Zeng, Y.; Zhao, Y.; Sánchez, S. *Nano Lett.* **2016**, *16*, 2860.

(4) (a) Soler, L.; Magdanz, V.; Fomin, V. M.; Sánchez, S.; Schmidt, O. G. *ACS Nano* **2013**, *7*, 9611. (b) Parmar, J.; Vilela, D.; Pellicer, E.; Esqué-de los Ojos, D.; Sort, J.; Sánchez, S. *Adv. Funct. Mater.* **2016**, *26*, 4152.

(5) (a) Solovev, A. A.; Sánchez, S.; Pumera, M.; Mei, Y. F.; Schmidt, O. G. *Adv. Funct. Mater.* **2010**, *20*, 2430. (b) Restrepo-Perez, L.; Soler, L.; Martinez-Cisneros, C.; Sánchez, S.; Schmidt, O. G. *Lab Chip* **2014**, *14*, 2914.

(6) Wu, Z.; Wu, Y.; He, W.; Lin, X.; Sun, J.; He, Q. *Angew. Chem., Int. Ed.* **2013**, *52*, 7000.

(7) (a) Wu, J.; Balasubramanian, S.; Kagan, D.; Manesh, K. M.; Campuzano, S.; Wang, J. *Nat. Commun.* **2010**, *1*, 36. (b) Singh, V. V.; Kaufmann, K.; Esteban-Fernandez de Avila, B.; Uygun, M.; Wang, J. *Chem. Commun.* **2016**, *52*, 3360. (c) Orozco, J.; García-Gradilla, V.; D'Agostino, M.; Gao, W.; Cortés, A.; Wang, J. *ACS Nano* **2013**, *7*, 818.

(8) (a) Solovev, A. A.; Xi, W.; Gracias, D. H.; Harazim, S. M.; Deneke, C.; Sánchez, S.; Schmidt, O. G. *ACS Nano* **2012**, *6*, 1751. (b) Gao, W.; Dong, R.; Thamphiwatana, S.; Li, J.; Gao, W.; Zhang, L.; Wang, J. *ACS Nano* **2015**, *9*, 117.

(9) (a) Gao, W.; Sattayasamitsathit, S.; Orozco, J.; Wang, J. *J. Am. Chem. Soc.* **2011**, *133*, 11862. (b) Solovev, A. A.; Mei, Y. F.; Urena, E. B.; Huang, G. S.; Schmidt, O. G. *Small* **2009**, *5*, 1688.

(10) Mei, Y. F.; Huang, G. S.; Solovev, A. A.; Urena, E. B.; Moench, I.; Ding, F.; Reindl, T.; Fu, R. K. Y.; Chu, P. K.; Schmidt, O. G. *Adv. Mater. (Weinheim, Ger.)* **2008**, *20*, 4085.

(11) Safdar, M.; Wani, O. M.; Jänis, J. *ACS Appl. Mater. Interfaces* **2015**, *7*, 25580.

(12) Sánchez, S.; Solovev, A. A.; Mei, Y.; Schmidt, O. G. *J. Am. Chem. Soc.* **2010**, *132*, 13144.

(13) Harazim, S. M.; Xi, W.; Schmidt, C. K.; Sánchez, S.; Schmidt, O. G. *J. Mater. Chem.* **2012**, *22*, 2878.

(14) (a) Yao, K.; Manjare, M.; Barrett, C. A.; Yang, B.; Salguero, T. T.; Zhao, Y. *J. Phys. Chem. Lett.* **2012**, *3*, 2204. (b) Zhao, G. J.; Ambrosi, A.; Pumera, M. *J. Mater. Chem. A* **2014**, *2*, 1219. (c) Li, J.; Liu, Z.; Huang, G.; An, Z.; Chen, G.; Zhang, J.; Li, M.; Liu, R.; Mei, Y. *NPG Asia Mater.* **2014**, *6*, e94.

(15) Sánchez, S.; Solovev, A. A.; Harazim, S. M.; Deneke, C.; Feng Mei, Y.; Schmidt, O. G. *Chem. Rec.* **2011**, *11*, 367.

(16) (a) Schattling, P.; Thingholm, B.; Städler, B. *Chem. Mater.* **2015**, *27*, 7412. (b) Dey, K. K.; Zhao, X.; Tansi, B. M.; Méndez-Ortiz, W. J.; Córdova-Figueroa, U. M.; Golestanian, R.; Sen, A. *Nano Lett.* **2015**, *15*, 8311. (c) Bunea, A.-I.; Pavel, I.-A.; David, S.; Gáspár, S. *Biosens. Bioelectron.* **2015**, *67*, 42. (d) Abdelmohsen, L. K. E. A.; Nijemeisland, M.; Pawar, G. M.; Janssen, G.-J. A.; Nolte, R. J. M.; van Hest, J. C. M.; Wilson, D. A. *ACS Nano* **2016**, *10*, 2652. (e) Ma, X.; Wang, X.; Hahn, K.; Sánchez, S. *ACS Nano* **2016**, *10*, 3597. (f) Ma, X.; Jannasch, A.; Albrecht, U.-R.; Hahn, K.; Miguel-López, A.; Schäffer, E.; Sánchez, S. *Nano Lett.* **2015**, *15*, 7043. (g) Pantarotto, D.; Browne, W. R.; Feringa, B. L. *Chem. Commun.* **2008**, *10*, 1533.

(17) Spagnolie, S. E.; Lauga, E. *Phys. Fluids* **2010**, *22*, 081902.

(18) Yin, Y.; Lu, Y.; Sun, Y.; Xia, Y. *Nano Lett.* **2002**, *2*, 427.

(19) Tirado, M. M.; Martínez, C. L.; de la Torre, J. G. *J. Chem. Phys.* **1984**, *81*, 2047.

(20) Wang, X.; In, M.; Blanc, C.; Nobili, M.; Stocco, A. *Soft Matter* **2015**, *11*, 7376.

(21) Sengupta, S.; Patra, D.; Ortiz-Rivera, I.; Agrawal, A.; Shklyaev, S.; Dey, K. K.; Córdova-Figueroa, U.; Mallouk, T. E.; Sen, A. *Nat. Chem.* **2014**, *6*, 415.

(22) Happel, J.; Brenner, H. *Low Reynolds Number Hydrodynamics*, 2nd ed.; Martinus Nijhoff Publishers: The Hague, 1983.

(23) Wang, W.; Castro, L. A.; Hoyos, M.; Mallouk, T. E. *ACS Nano* **2012**, *6*, 6122.

DOI: 10.1021/jacs.6b06857
J. Am. Chem. Soc. 2016, 138, 13782−13785